Vertically Aligned Dense Carbon Nanotube Growth with Diameter Control by Block Copolymer Micelle Catalyst Templates

ARTICLE *in* THE JOURNAL OF PHYSICAL CHEMISTRY B · NOVEMBER 2006

Impact Factor: 3.3 · DOI: 10.1021/jp0647378 · Source: PubMed

5 AUTHORS, INCLUDING:

Alan M Cassell
NASA
139 PUBLICATIONS **10,506** CITATIONS
SEE PROFILE

Brett A. Cruden
NASA
102 PUBLICATIONS **1,769** CITATIONS
SEE PROFILE

THE JOURNAL OF PHYSICAL CHEMISTRY B LETTERS

2006, *110*, 20102−20106
Published on Web 09/19/2006

Vertically Aligned Dense Carbon Nanotube Growth with Diameter Control by Block Copolymer Micelle Catalyst Templates

Xi Liu, Terry P. Bigioni, Yuan Xu,† Alan M. Cassell, and Brett A. Cruden*

Center for Nanotechnology, NASA Ames University Affiliated Research Center, NASA Ames Research Center, Mail Stop 223-2, Moffett Field, California 94035

Received: July 25, 2006; In Final Form: August 22, 2006

We have grown a dense array of vertically aligned carbon nanotubes (CNTs) with a controlled distribution of diameters by using block copolymer micelles to form and pattern catalyst particles. The block copolymer poly(styrene-*block*-acrylic acid) (PS_{16500}−PAA_{4500}) was dissolved in toluene to form micelles and then loaded with $FeCl_3$. The metal-loaded micelles were spin-coated on Si and then thermally treated to remove the polymer. Using this process, we produced surfaces patterned with iron oxide catalyst particles with particle densities ranging from 1400 μm^{-2} to 3800 μm^{-2} and a size distribution of (6.9 ± 0.8) nm. CNT growth by thermal chemical vapor deposition was then performed on these samples. The low-density catalyst sample produced unaligned, low-density CNTs, whereas the high-density catalyst sample produced vertically aligned, dense CNTs about 10 μm in length. Transmission electron microscopy revealed that the CNTs typically had double and triple graphitic layers with normally distributed diameters of (4.5 ± 1.1) nm. For comparison, CNTs grown from the standard approach of blanket Fe films had a wide distribution of diameters between 6 and 21 nm. This catalyst preparation approach dramatically sharpens the size distribution of CNTs, compared to standard approaches, and provides a simple means of controlling the areal density of CNTs.

Vertically aligned carbon nanotubes (CNTs) are key platforms for many potential applications, such as thermal interface materials,[1] microelectronics,[2] and flat panel displays.[3] For applications where CNTs must be bound to a substrate, chemical vapor deposition (CVD) is typically employed. In this method, a metal thin film is first evaporated on the substrate. Then, at high temperature, the film breaks apart and forms the metal particles as the catalyst for carbon nanotube growth.[4] The disadvantage of this method is that it is very difficult to control uniformity of catalyst size and growth density. Many research groups are focused on directly tuning the spacing and size of catalyst particles by different methods,[5−12] such as pulse-current electrochemical deposition, electron-beam lithography, shadow mask, and wet chemical methods.

Block copolymers have also been used extensively as self-assembled templates for the preparation of periodic nanoparticle arrays. The choice of diblock copolymer not only determines the size of the nanoparticles, but it also determines the particle−particle spacing and therefore the areal density of catalyst particles. Self-assembly of particles onto the substrate also provides a low-cost alternative to thin film deposition approaches such as sputtering and evaporation. This approach has been applied successfully to Au nanoparticle formation using polystyrene−poly(2-vinyl pyridene) (PS−P2VP) and other similar block copolymers.[13−16] Although some of these works have claimed formation of other metal particles using aprotic salts, we have found that the commercially available aprotic ionic metal salts relevant for CNT growth did not dissolve well in the P2VP micelle. Boontongkong and Cohen[17] demonstrated that the amphiphilic block copolymer polystyrene−poly(acrylic acid) (PS−PAA) effectively loaded these ionic metal salts into the PAA core. Bennett et al.[18] used iron-loaded PS−PAA, and Hinderling et al.[19] used iron-loaded polystyrene-*b*-poly(ferrocenyldimethylsilane) (PS−PFS) as templates to produce CNTs by thermal CVD. Although they had CNT growth, no vertically aligned CNT arrays were reported.

In this letter, we report the formation of Fe containing micelles of uniform size and Fe content. These micellar catalyst particles can then be patterned, with varying areal density, onto a Si substrate for the thermal growth of CNTs. Our results show that the narrow size distribution of the catalyst particles is reflected in the diameters of the CNTs and suggest that there is a minimum areal density of catalyst particles in order to achieve vertically aligned carbon nanotube growth.

Methods for preparing metal-loaded PS−PAA micelles have been described elsewhere.[10] For our experiments, PS−PAA diblock copolymer, with molecular weights of PS = 16 500 g/mol and PAA = 4500 g/mol, was dissolved in toluene with a concentration of 12 mg/mL and stirred for 4 h. The solution appeared slightly cloudy, indicating the presence of the cylindrical phase as described in ref 10. To convert all of the polymer material to the spherical micelle phase, the solution was heated to 150 °C for 20 min and then cooled to room temperature.[18] $FeCl_3$ was then added to the solution with a 3:1 PAA monomer/Fe mole ratio, as this reflects the charge ratio of the acrylic acid monomer to the iron cation. The color of the micelle solution changed to dark yellow when the iron salts were added. The Fe-loaded solution was then divided into five parts, shown in Table 1, where solutions A, B, and C were diluted to

† Nanoconduction, Inc. 1244 Reamwood Ave., Sunnyvale, CA 94089.

10.1021/jp0647378 CCC: $33.50

TABLE 1: Details of the Solutions

solution	casting method	concentration (mg/mL)	thickness (nm)	full surface coverage	density[a] ($/\mu m^2$)
A	spin[b]	1.8	~32	no	1400[c]
B	spin[b]	3.6	~34	yes	1400
C	spin[b]	7.2	~90	yes	3000
D	spin[b]	12	~90	yes	3800
E	dip[d]	12	~30	yes	1400

[a] Particle density counted after polymer thermally removed. [b] Spin speed at 1600 rpm for 1 min. [c] Particle analysis excluding the vacancy area. [d] Dip-casting withdrawal speed 10 mm/min.

concentrations of 1.8, 3.6, and 7.2 mg/mL, respectively, and solutions D and E were kept at 12.0 mg/mL. Solutions A−D were spin-coated at 1600 rpm for 1 min onto Si(100) with a native oxide layer. Solution E was dip-coated onto the same type of substrate with a withdrawal rate of 10 mm/min. The micelle films were then heated in air to 400 °C for 2 h to remove the polymer, leaving iron oxide[20] particles on the Si substrate. After cleaving, the typical sample size is about 1 cm × 1 cm.

Thermal CVD was carried out in a 200 mm Applied Materials P5000 CVD system that has been modified for CNT growth. Two Fe catalyst systems, the aforementioned iron oxide particles from micelle solutions and a 5 nm sputtered Fe blanket film, were used for CNT growth under the same growth conditions. The samples were transferred in air under room temperature to the growth chamber where they were heated on a Mo plate to 600 °C. Ammonia was introduced to pretreat the samples for 5 min, and then the substrate heater temperature was increased to a target temperature of 780 °C for growth. During the 8 min growth period, the flows of C_2H_4 and NH_3 were kept constant at 100 and 200 sccm under a total pressure of 4 Torr. Once the growth was complete, the samples were immediately moved to another vacuum chamber to cool to room temperature before exposure to air.

A Hitachi 4800 scanning electron microscope (SEM) was used to characterize the iron oxide particles and CNTs. Images of the CNT structure were taken with a JEOL 2010 high-resolution transmission electron microscope (HRTEM). CNTs were dispersed onto Cu TEM grids for HRTEM analysis. An X-ray photoelectron spectrometer (XPS) was used for surface elemental analysis. Thicknesses of the polymer films were measured by both SEM and atomic force microscopy. Particle density and size distribution analyses were done using *ImageJ*.[21]

Film thinning during spin-coating results from the combination of convective radial outflow, driven by the centrifugal force of spinning, and solvent evaporation. Thus, the film thickness depends on many variables such as spin speed, solvent evaporation rate, and polymer concentration. Our results in Table 1 show that solutions with higher initial concentrations produce thicker films than solutions with lower concentrations.[22] For dip-coated substrates, the withdrawal rate is the most common parameter used to control the film thickness. However, we found that monolayer coverage was always obtained for withdrawal rates between 5 and 200 mm/min. Therefore, only one dip-coated sample with a withdrawal speed of 10 mm/min in solution E is presented in Table 1, with a film thickness of ~30 nm and final particle density of $1400/\mu m^2$.

Using solutions A−D, with concentrations of 1.8, 3.6, 7.2, and 12 mg/mL, we spin-coated films with nominal thicknesses of ~32, ~34, ~90, and ~90 nm, respectively. At the lowest concentration, the surface coverage was below ~66%, while a concentration of 3.6 mg/mL resulted in monolayer coverage across the entire surface. Because of the tendency for PS−PAA micelles to self-assemble on the substrate, these films formed as quasi-hexagonal monolayer arrays, as shown in Figure 1. These arrays retained their structure even after thermal processing. Both films had a particle density of $1400/\mu m^2$ in the regions covered by particles (Table 1). The thickness of these films is consistent with the center-to-center spacing of the micelles and the expected micelle diameter, as expected for a close-packed monolayer. Previous results showed similar arrays with particle densities of $\sim 1000/\mu m^2$ and center-to-center spacings of about 30−35 nm.[18]

For the thicker films, the particle densities were higher. These films had particle densities of $3000/\mu m^2$ and $3800/\mu m^2$ for the 7.2 mg/mL and 12 mg/mL concentrations, respectively. This demonstrates that the final particle density can be controlled by adjusting the initial concentrations of the micelle solutions. Both films had measured thicknesses of 90 nm, consistent with a close-packed trilayer film of micelles. It is interesting to note

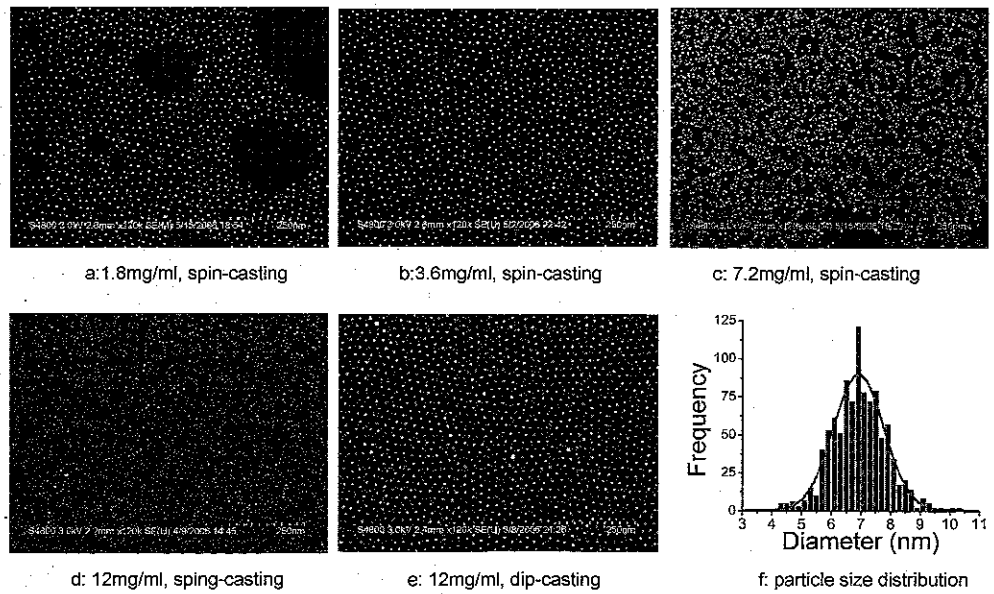

Figure 1. SEM images of iron oxide particles from different concentrations of solutions A, B, C, and D from spin-casting (a−d) and solution E from dip-casting (e) after thermally removing the polymer (all scale bars are 250 nm). (f) is a histogram of particle sizes from (b) with a diameter distribution of 6.9 ± 0.8 nm.

that films consistent with a bilayer were not observed, though presumably this could be achieved at intermediate concentrations.

Figure 1a–e shows SEM images of the iron oxide particles formed from the different solutions after thermally removing the polymer (a–d from spin-casting and e from dip-casting). Figure 1f is a histogram of particle diameters, with a size distribution of 6.9 ± 0.8 nm. Particles deposited at concentrations of 3.6 mg/mL and above (Figure 1b–d) demonstrate complete coverage of the substrates, while particles deposited from a 1.8 mg/mL solution (Figure 1a) give incomplete surface coverage. The higher concentration solutions form multilayer films under these spin-casting conditions but have the same diameter distribution (histogram not shown). The fact that the diameter distributions are identical for all cases implies that the particle size is determined by the micelle dimensions and is not influenced by the concentration of micelles in solution, as expected. In all cases, the diameter distribution is normally distributed.

Particles deposited as a monolayer film, in Figure 1b, show regular ordering (center-to-center spacing ~30 nm) with a particle density of 1400/μm^2. Particles deposited as a multilayer film, in Figure 1d, have less ordering and a higher particle density of 3800/μm^2. After removal of the polymer, we believe that the particles in the upper layers come to reside in the interstitial regions of the first layer. This increases the particle density and also reduces the ordering of the particles, as observed. For trilayer coverage, as the thickness measurements indicated, one would expect the particle density to be three times that of the monolayer; however, it is slightly less than three times that of the monolayer coverage. This indicates that the multilayered films may have a more disordered arrangement than the monolayer or that the second and third layers are not completely filled.

Previous work[18] using low-density particles (~1000/μm^2) showed sparse and randomly oriented CNTs after 60 min of growth. These results might be due to the choice of growth conditions, density of the catalyst particles, purity of the particles, or a combination of all three of these. In our case, thermal growth using the dip-coated low-density particles (~1400/μm^2) resulted in low-density, randomly oriented growth of CNTs, as shown in Figure 2a. Using the higher density (3800/μm^2) particles and the same growth conditions, we were able to demonstrate high-density growth, as shown in Figure 2b. After 8 min of growth, the CNTs were dense and vertically aligned with a mean length of ~10 μm. Alignment of this nature has been demonstrated by several other authors using blanket films, as in Figure 2c, and is believed to be due to steric crowding of neighboring nanotubes, alternatively interpreted as a van der Waals effect.[7] On the basis of these prior studies, it is reasonable to attribute the alignment to the high-density patterning. There is presumably a critical density required for achieving vertical alignment; however, this has not been reported in the literature and is likely dependent on the growth conditions and reactor. Still, other factors such as variation in catalyst activity should not be discounted in explaining this result.

At low coverage, the catalyst activity appears to be less than 20%. At high coverage, it is difficult to tell what the activity is. Two mechanisms that could affect the catalyst activity are the purity of the particles or microloading. Impurities that could adversely affect growth include silicide or carbide formation during the burning process or incomplete reduction of the oxide during pretreatment. However, there is no obvious reason to believe these properties to be different for the sparse case than the dense case. Microloading, where the chemical species present at the surface are altered by catalytic surface reactions when the catalyst density is high, may result in a higher activity for dense catalyst films. This phenomenon has been observed previously where areas of high catalyst density have a higher activity than regions of low density.[23] Therefore, the higher coverage may give a greater catalyst activity in addition to a higher density of catalyst sites.

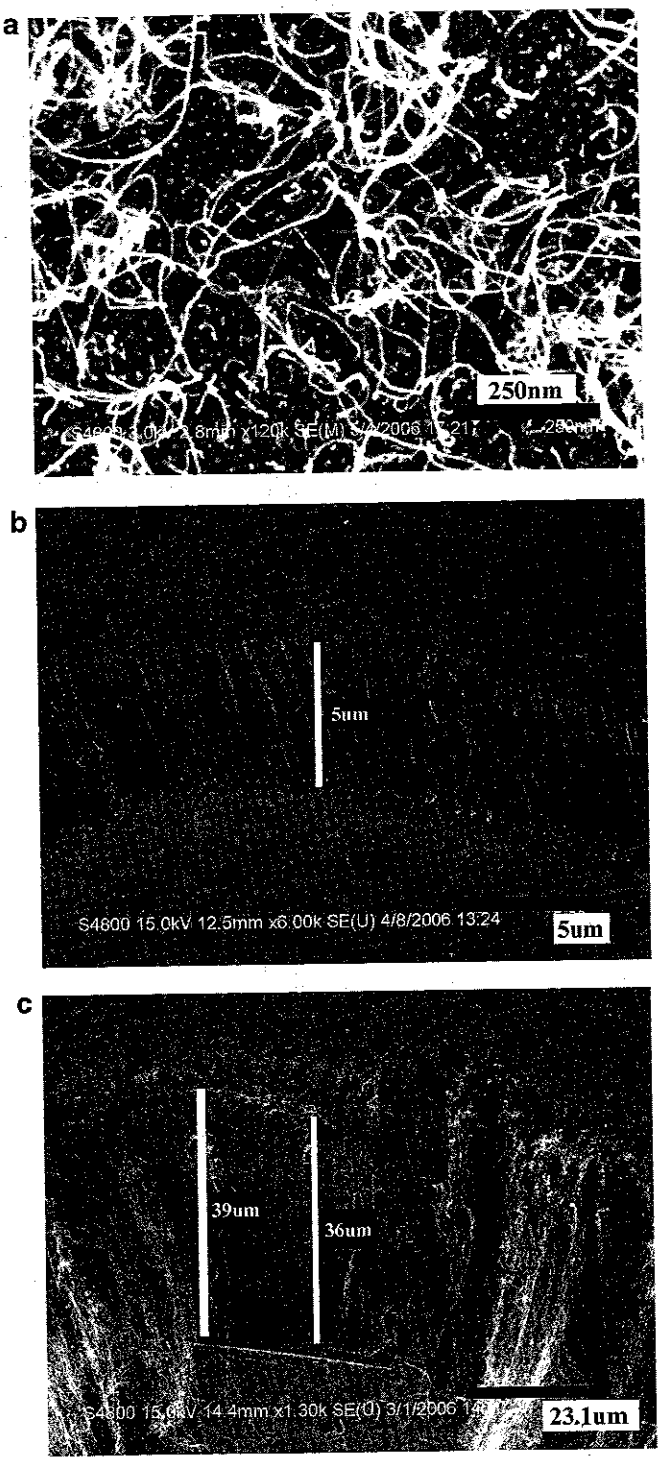

Figure 2. SEM images of CNTs on Si (30° tilt angle), grown from (a) low-density particles (1400/μm^2), (b) high-density particles (3800/μm^2), and (c) 5 nm blanket iron film. Scale bars are 250 nm in (a), 5 μm in (b), and 23.1 μm in (c).

Figure 3a shows a HRTEM image of the vertical aligned CNTs. Figure 3c is the diameter distribution obtained by analysis of several such images. HRTEM images show that the CNTs

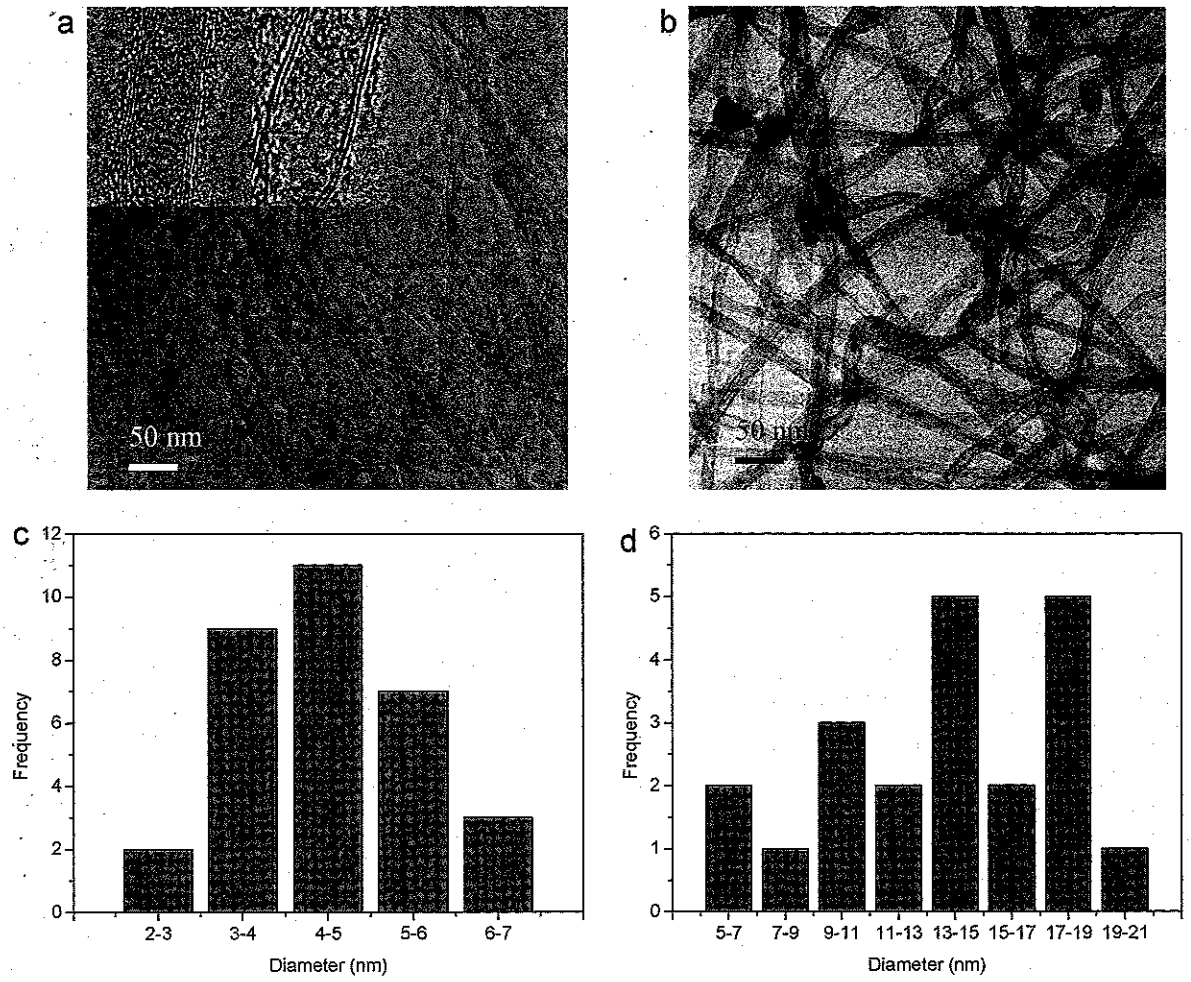

Figure 3. TEM images of CNTs grown from (a) iron particles (insets: high-resolution image showing two and three walls), (b) 5 nm blanket iron film in thermal CVD chamber under the same growth conditions. (c) and (d) are CNT diameter histograms for (a) and (b), respectively.

are typically double- and triple-walled tubes with a mean diameter of 4.5 ± 1.1 nm. Assuming the catalyst particles imaged after calcination are uniform spheres of γ-Fe_2O_3, full reduction to metallic Fe would decrease the size distribution to 5.4 ± 0.7 nm. The average ratio of diameter of catalyst particles to CNT is then 1.2, which is similar to that found by other authors.[24] However, prior TEM characterization of these nanoparticles has shown a void space in the center of the particle.[17] A densified iron particle diameter could be estimated from the PAA-monomer-to-iron-atom ratio. Assuming the micelle inner diameter to be 6.9 nm and density to be 1.0 g/cm^3 would give an iron particle density of 4.4 nm, putting the ratio closer to 1. It is interesting to note that the CNT diameter distribution is wider than the catalyst distribution, which may be attributed to a coarsening of particle size during heat treatment. Indeed, imaging the catalyst after thermal treatment did appear to display some coarsening, and a small amount of larger-diameter tubes were observed in TEM.

For comparison, a sputtered 5 nm thin film of iron was used to grow CNTs under the same conditions, as shown in Figure 2c. Figure 3c shows an HRTEM image of CNTs from the blanket Fe film. Although the blanket film produced vertically aligned growth, the diameter distribution of the CNTs was much broader and not normally distributed, as shown in Figure 3d. The CNTs from the blanket film have a flat diameter distribution ranging from 6 to 21 nm with a mean diameter of 13.5 nm and a standard deviation of 3.9 nm. It was not always possible to discern the number of walls in these tubes, but as few as 6 to as many as 16 walls were observed. It appears that this stochastic mechanism of nanoparticle formation results in an essentially random distribution of catalyst particles and hence a flat nanotube diameter distribution. However, the flatness of this distribution may in part be due to the limited number of samples characterized to obtain the distribution. Regardless, it is clear that the micelle patterning approach used here provides far more control over CNT diameter distributions than does growth from a blanket film.

These vertically aligned CNTs are weakly adhered to the Si surface and, as a result, are very easily peeled off. A similar weak adhesion with peelable films has been observed by other authors.[25,26] While Bennett et al.[18] were unable to unambiguously determine their growth mechanism, we can use this weak adhesion to identify our growth mechanism. The fact that we can peel off the CNT film allows us to examine the surface for iron particles remaining on the substrate. Indeed, both SEM and XPS data (not shown) confirm that Fe-containing particles are left behind on the substrate, indicating that our growth mechanism is base growth. These results indicate that the adhesion between nanotubes and catalyst particles is quite poor in these systems. However, this type of adhesive failure is not common to all nanotube catalyst formulations, and the reasons behind this are not yet well-understood.

In conclusion, we have demonstrated the ability to synthesize iron-loaded diblock micelles, pattern them on a surface, and then use them to grow vertically aligned carbon nanotubes by low-pressure CVD. We have demonstrated that catalyst densities can be controlled simply by varying the concentration of the spin-cast micellar solution, achieving catalyst particle densities

of up to ~3800/μm^2. These high-density films were used to successfully grow vertically aligned two- and three-walled CNTs by the base growth mechanism. The CNTs grown by this micellar catalyst method were found to have a narrow, normally distributed diameter distribution. In comparison, CNTs grown from a blanket film catalyst had a wide range of diameters. This micelle patterning method represents a substantial improvement over traditional catalyst preparation approaches by allowing a degree of diameter and density control that is otherwise unattainable.

Acknowledgment. The authors would like to acknowledge support by the UC Discovery Grant and the Industry−University Cooperative Research Program. This research made use of Nanoconduction, Inc., facilities. We would also like to thank Mr. Gary Schulz for SEM characterization, Mr. Rahim Kavari and Ms. Lydia Lujan for CNT growth, and Ms. Ru Yan for helpful statistical discussions.

References and Notes

(1) Ngo, Q.; Cruden, B. A.; Cassell, A. M.; Sims, G.; Meyyappan, M.; Li, J.; Yang, C. Y. *Nano Lett.* **2004**, *4*, 2403.

(2) Graham, A. P.; Duesberg, G. S.; Seidel, R. V.; Liebau, M.; Unger, E.; Pamler, W.; Kreupl, F.; Hoenlein, W. *Small* **2005**, *1*, 382.

(3) Kuttel, O. M.; Groening, O.; Emmenegger, C.; Schlapbach, L. *Appl. Phys. Lett.* **1998**, *73*, 2113.

(4) Hofmann, S.; Ducati, C.; Robertson, J.; Kleinsorge, B. *Appl. Phys. Lett.* **2003**, *83*, 135.

(5) Tu, Y.; Huang, Z. P.; Wang, D. Z.; Wen, J. G.; Ren, Z. F. *Appl. Phys. Lett.* **2002**, *80*, 4018.

(6) Javey A.; Dai, H. *J. Am. Chem. Soc.* **2005**, *127*, 11942.

(7) Fan, S.; Chapline, M. G.; Franklin, N. R.; Tombler, T. W.; Cassell, A. M.; Dai, H. *Science* **1999**, *283*, 512.

(8) Cheung, C. L.; Kurtz, A.; Park, H.; Lieber, C. M. *J. Phys. Chem. B* **2002**, *106*, 2429.

(9) Fu, Q.; Huang, S.; Liu, J. *J. Phys. Chem. B* **2004**, *108*, 6124.

(10) Bennett, R. D.; Miller, A. C.; Kohen, N. T.; Hammond, P. T.; Irvine, D. J.; Cohen, R. E. *Macromolecules* **2005**, *38*, 10728.

(11) Ago, H.; Ohshima, S.; Uchida, K.; Komatsu, T.; Yumura, M. *Physica B* **2002**, *323*, 306.

(12) Amama, P. B.; Maschmann, M. R.; Fisher, T. S.; Sands, T. D. *J. Phys. Chem. B* **2006**, *110*, 10636.

(13) Spatz, J. P.; Mossmer, S.; Hartmann C.; Moller, M., Herzog, T.; Krieger, M.; Boyen, H. G.; Ziemann, P.; Kabius, B. *Langmuir* **2000**, *16*, 407.

(14) Liu, X.; Jaramillo, T.; Kolmakov, A.; Baeck, S. H.; Moskovits, M.; Stucky, G. D.; McFarland, E. W. *J. Mater. Res.* **2005**, *20*, 1093.

(15) Sidorov, S. N.; Bronstein, L. M.; Kabachii, Y. A.; Valetsky, P. M.; Soo, P. L.; Maysinger, D.; Eisenberg, D. *Langmuir* **2004**, *20*, 3543.

(16) Spatz, J. P.; Roescher, A.; Moller, M. *Adv. Mater.* **1996**, *8*, 337.

(17) Boontongkong, Y.; Cohen, R. E. *Macromolecules* **2002**, *35*, 3647.

(18) Bennett, R. D.; Xiong, G. Y.; Ren, Z. F.; Cohen, R. E. *Chem. Mater.* **2004**, *16*, 5589.

(19) Hinderling, C.; Keles, Y.; Stockli, T.; Knapp, H. F.; Arcos, T.; Oelhafen, P.; Korczagin, I.; Hempenius, M. A.; Vancso, G. J.; Pugin, R.; Heinzelmann, H. *Adv. Mater.* **2004**, *16*, 876.

(20) Garcia, C.; Zhang, Y.; DiSalvo, F.; Wiesner, U. *Angew. Chem., Int. Ed.* **2003**, *42*, 1526.

(21) ImageJ. http://rsb.info.nih.gov/ij/ (accessed July 2006).

(22) Yimsiri P.; Mackley, M. R. *Chem. Eng. Sci.* **2006**, *61*, 3496.

(23) Cassell, A. M.; Ye, Q.; Cruden, B. A.; Ng, H. T.; Li, J.; Han, J.; Meyyappan, M. *Nanotechnology* **2004**, *15*, 9.

(24) Nasibulin, A. G.; Pikhitsa, P. V.; Jiang, H.; Kauppinen, E. I.; *Carbon* **2005**, *43*, 2251.

(25) Hata, K.; Futaba, D. N.; Mizuno, K.; Namai, T.; Yumura, M.; Iijima, S. *Science* **2004**, *306*, 1362.

(26) Zhang, G. Y.; Mann, D.; Zhang, L.; Javey, A.; Li, Y. M.; Yenilmez, E.; Wang, Q.; McVittie, J. P.; Nishi, Y.; Gibbons, J.; Dai, H. J. *Proc. Natl. Acad. Sci. U.S.A.* **2005**, *102*, 16141.